THE JOURNAL OF PHYSICAL CHEMISTRY Letters

Letter

Cite This: J. Phys. Chem. Lett. 2019, 10, 2170−2174

pubs.acs.org/JPCL

Peptide-Controlled Assembly of Macroscopic Calcium Oxalate Nanosheets

Hao Lu,*[,†] Arne Schäfer,[†] Helmut Lutz,[†] Steven J. Roeters,[§] Ingo Lieberwirth,[†] Rafael Muñoz-Espí,[‡] Matthew A. Hood,[†] Mischa Bonn,[†] and Tobias Weidner[†,§]

[†]Max Planck Institute for Polymer Research, Ackermannweg 10, 55128 Mainz, Germany

[‡]Institute of Materials Science (ICMUV), Universitat de València, C/Catedràtic José Beltrán 2, 46980 Paterna, Spain

[§]Department of Chemistry, Aarhus University, Langelandsgade 140, 8000 Aarhus C, Denmark

Supporting Information

ABSTRACT: The fabrication of two-dimensional (2D) biomineral nanosheets is of high interest owing to their promise for applications in electronics, filtration, catalysis, and chemical sensing. Using a facile approach inspired by biomineralization in nature, we fabricate laterally macroscopic calcium oxalate nanosheets using β-folded peptides. The template peptides are composed of repetitive glutamic acid and leucine amino acids, self-organized at the air−water interface. Surface-specific sum frequency generation spectroscopy and molecular dynamics simulations reveal that the formation of oxalate nanosheets relies on the peptide−Ca^{2+} ion interaction at the interface, which not only restructures the peptides but also templates Ca^{2+} ions into a calcium oxalate dihydrate lattice. Combined, this enables the formation of a critical structural intermediate in the assembly pathway toward the oxalate sheet formation. These insights into peptide−ion interfacial interaction are important for designing novel inorganic 2D materials.

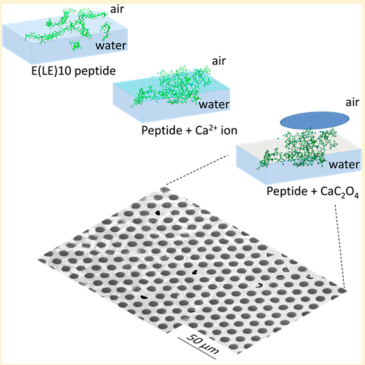

The design and synthesis of 2D nanomaterials have opened up a new field of ultrathin, functional materials with atomic precision.[1] Organic sheet materials such as graphene have received much attention recently. Inorganic 2D nanomaterials composed of metal oxides, ceramics, and minerals also hold great promise as materials with new physical and chemical properties, which can be chemically tuned and self-assembled using effective, low-cost, bottom-up fabrication methods.[2] Synthesized from relatively cheap building blocks, such materials offer great flexibility in tailoring surface morphology, porosity, chemical functionality, and electronic properties. One particularly interesting strategy to obtain functional 2D inorganic materials has been their templated assembly via organic precursor structures. Here, the chemical and polymorph structure can be encoded in the chemistry and structure of the organic templating layer. Nature uses this mechanism with proteins, which "engineer" intricately mineralized tissue by steering the growth of minerals and thereby achieving polymorph and shape control in, e.g., bone and teeth[3] and exoskeletons of mollusks or diatoms.[4] Over the past years, researchers have therefore been taking clues from Nature in an attempt to mimic the control that specialized biomolecules involved in hard tissue biogenesis exert over the formation of inorganic layered materials. Despite the great efforts, biomimetic fabrication of 2D inorganic materials still largely relies on trial and error and, therefore, typically requires substantial investments of time and funds.

Surfactants,[5] lipids,[6] peptoids,[7,8] and polymers[9] have been reported to grow 2D organic sheets. Such structures can potentially steer the growth of biomimetic mineral nanosheets at interfaces, such as the air−water[10] or oil−water interfaces,[8] into desired polymorphs and morphologies. Solid-supported layers have also been used for the synthesis of layered materials.[1] Oxide and ceramic materials are particularly interesting in this context for the assembly of electronic circuitry, semiconductors, photonic materials, as well as nanometer thin membranes for desalination, filtration, chemical separation, catalytic applications, and sensors. For biomedical or nanofabrication applications, biomineral nanosheets have been explored recently.[2,10,11] In particular, calcium carbonate and calcium oxalate (CaC_2O_4) are versatile biocompatible materials, which are chemically and structurally extremely stable.

The synthesis of extended calcium carbonate sheets using biomolecules as organic templates has recently been reported.[10] In contrast, CaC_2O_4, the dominant part of kidney stones[12,13] and notoriously stable, has largely remained unexplored as a functional material. Despite the extraordinary stability and inertness of CaC_2O_4, for, e.g., coatings to protect marble and archeological monuments from environmental degradation,[14] CaC_2O_4 precipitation studies have remained limited to particles and bulk solids; applications for 2D nanomaterials have thus far not been exploited.

Received: March 11, 2019
Accepted: April 12, 2019
Published: April 12, 2019

DOI: 10.1021/acs.jpclett.9b00684
J. Phys. Chem. Lett. 2019, 10, 2170−2174

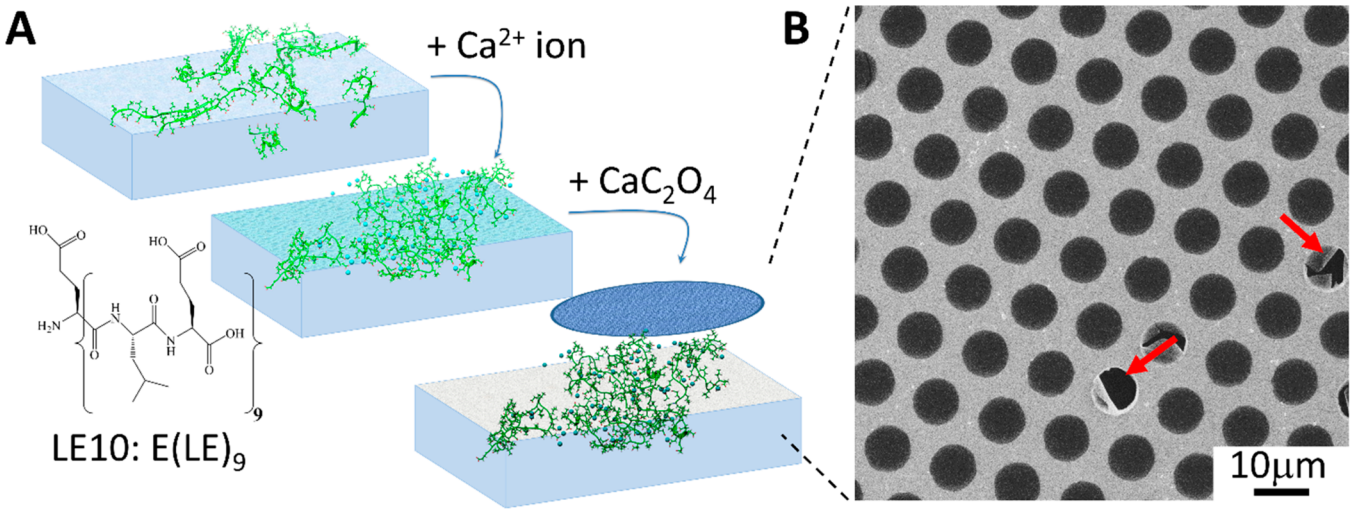

Figure 1. (A) LE10 peptide-mediated surface nucleation of CaC_2O_4 nanosheets. The sheets can be lifted off from the water surface with a TEM grid. (B) SEM image of a LE10 templated CaC_2O_4 sheet collected from the air−water interface using a TEM copper grid. Red arrows indicate the broken part of the sheet; defect-free sheets over 50 × 50 μm^2 can routinely be achieved.

To investigate the potential of CaC_2O_4 biominerals as a 2D material, we report here the synthesis of CaC_2O_4 nanosheets at the air−water interface using biomimetic peptides (Figure 1A). Proteins that can effectively bind to a mineral surface are generally also effective nucleators of that mineral. Our choice of peptide for this experiment was inspired by the highly acidic human urinary protein osteopontin; it can specifically bind and passivate (CaC_2O_4) kidney stones and thereby avoid the growth of larger stones.[12,13] The peptide sequence NH_2−$E(LE)_9$−COOH (abbreviated as LE10, Figure 1A) used in this study mimics the high glutamic acid content of osteopontin and has been shown to organize into strand-like structures at the air−water interface,[10] reminiscent of binding sites in osteopontin. In a recent study, we found that β-folded leucine−glutamic acid (LE) peptides can effectively assemble vaterite calcium carbonate nanosheets by exploiting their structural flexibility at the air−water interface,[10] which prompts us to explore this designed LE10 sequence to fabricate a novel 2D nanomaterial based on calcium oxalate.

Indeed, CaC_2O_4 nanosheets can be achieved by mineralizing CaC_2O_4 using the template of assembled LE10 peptides at the air−water interface. Figure 1A illustrates the formation process of the CaC_2O_4 nanosheet: Firstly, the LE10 peptides were assembled at the air−water interface of a 20 mL trough filled with a 0.1 mg/mL solution of LE10 peptides. Upon surface adsorption, the subphase was diluted by a factor of 8 to reduce the bulk peptide concentration. Subsequently, calcium cations (Ca^{2+}) and oxalate anions ($C_2O_4^{2-}$) were injected into the subphase, this procedure led to CaC_2O_4 mineralization by LE10 peptides at the air−water interface. A thin layer of biomineral, consisting of mineral and peptides, could be lifted off of the interface with a transmission electron microscopy (TEM) grid. The scanning electron microscopy (SEM) image in Figure 1B shows that the CaC_2O_4 sheet extends over the entire grid and is without visible cracks or fractures over an area of 50 × 50 μm^2. The sheet is intact and freestanding over most of the grid holes where the film is without any support. The sheets shown in Figure 1B extend over several square millimeters across the TEM grid with comparable quality. It is challenging to retrieve the atomically resolved CaC_2O_4 crystal structure within the nanometer sheet from high-resolution TEM measurement, in particular, taking into account the fact that the CaC_2O_4 crystals are typically decomposed into the amorphous phase by interaction with high-energy electrons.[15] However, the observable diffuse rings from electron diffraction (Figure S3) suggests that the CaC_2O_4 crystals in the sheet are rather arranged into ordered nuclei prior to crystal growth, which is also in agreement with the nonclassic views of CaC_2O_4 mineralization.[15]

X-ray photoelectron spectroscopy (XPS) analysis indicates that the nanosheets have a thickness of ∼2 nm, and the elemental composition of the sheets (Table S1) reveals that each Ca^{2+} ion is shared by ∼2 glutamic acid side chains of peptides. No contaminants or unexpected elements were detected within the sheets. The XP spectra (Figure S1) are in agreement with those of hybrid CaC_2O_4/peptide sheets forming directly at the peptide interface. Combined, the SEM and XPS results clearly show that LE10 peptides grows 2D CaC_2O_4 nanosheets.

To elucidate the molecular mechanism underlying CaC_2O_4 nanosheet formation, we applied surface-specific sum frequency generation (SFG) spectroscopy. SFG is a second-order nonlinear spectroscopy, sensitive to ordered species exclusively at the interface.[16−19] This technique allows us to follow the molecular details of peptide arrangement, at the interface and in situ, during nanosheet formation. In our SFG measurement in the amide I region, D_2O was used as the solvent instead of H_2O to avoid spectral interference from H_2O bending modes. Figure 2A shows SFG spectra using an SPS (S-polarized SFG, P-polarized vis, S-polarized IR) polarization combination for LE10 peptides assembled at the air−water interface, at different times after Ca^{2+} ion ($CaCl_2$) injection, and after CaC_2O_4 mineralization ($Na_2C_2O_4$ injection). The chosen SPS polarization combination is sensitive to both backbone and Glu side chain modes.[10] The spectra of the pristine peptides exhibit two bands at ∼1576 and ∼1612 cm^{-1}, corresponding to the asymmetric COO^- stretching vibration from the deprotonated Glu side chains[20,21] and the B2 mode of the β-sheet backbone, respectively.[22,23] The presence of two distinct bands indicates that both peptide backbone and side chains are well ordered at the buffer−air interface. Both bands increase in intensity upon Ca^{2+} ion interaction: the side chain band

DOI: 10.1021/acs.jpclett.9b00684
J. Phys. Chem. Lett. 2019, 10, 2170−2174

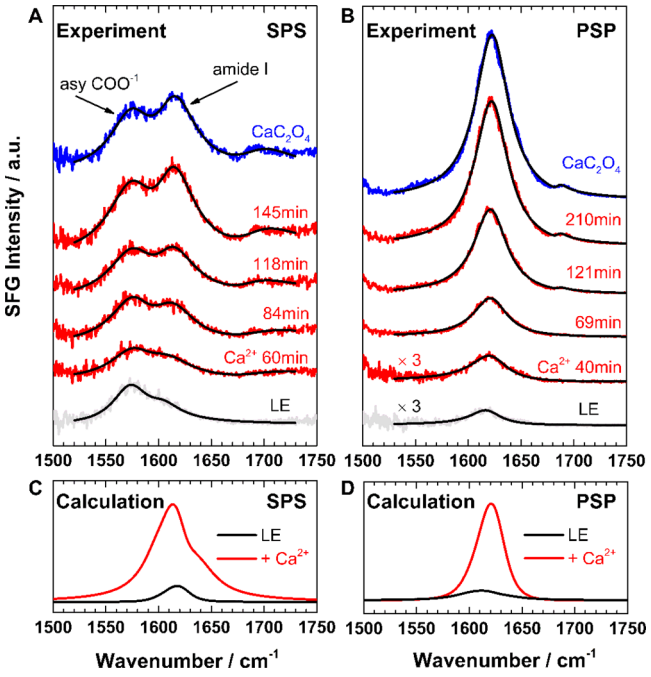

Figure 2. (A,B) Experimental SFG spectra in the amide I region for LE10 peptides at the air−water interface (gray), with Ca^{2+} ion interaction at different times after $CaCl_2$ injection (red), and following CaC_2O_4 mineralization (blue). The spectra were acquired under (A) achiral SPS and (B) chiral PSP polarization combinations. The fits (black) are superimposed onto the experimental data. (C,D) Calculated amide I SFG spectra for peptides before and after Ca^{2+} ion interaction agree well with experimental spectra.

increases slightly, while the backbone amide I peak increases drastically, to saturate after ∼3 h. The gradual amide I band increase indicates that the β-strands refold into more compact, ordered states. A weak feature at ∼1690 cm^{-1} appears after ∼2 h of Ca^{2+} ion interaction; this high-frequency band can be assigned to β-turn motifs in less folded peptide aggregates.[24] A detailed spectral analysis (Figure S6) reveals a slight frequency shift of the central amide I band from 1605 to 1612 cm^{-1} with time, possibly related to the couplings between the local modes of the turn motifs.

The backbone folding structure can be resolved in more detail using SFG spectra under chiral PSP polarization combinations (Figure 2B) that exclusively probe the amide bonds from β-folded peptides without spectral interference from achiral side chain modes.[25,26] As expected, those spectra show only the predominant chiral amide I peak centered at ∼1620 cm^{-1}, which originates from the β-sheet backbone,[26] while the side chain band lacking chirality is fully suppressed. In accordance with the SPS spectra in Figure 2A, the interaction with Ca^{2+} ions enhances the amide I intensity and gives rise to a shoulder at ∼1690 cm^{-1}, testifying to the peptide backbones refolding into more ordered, compact β-turns.

The SFG results provide direct experimental proof of peptide refolding upon interaction with Ca^{2+} ions—a key step for CaC_2O_4 sheet formation. For a molecular picture visualizing the critical assembled intermediate of peptides and Ca^{2+} ions, we performed molecular dynamics (MD) simulations for LE10 peptides in the absence and presence of Ca^{2+} ions. Snapshots in Figure 3A show the strand-like assembly of LE10 in the absence of Ca^{2+} ions. This secondary structure is also expected based on folding of the analogue positively charged leucine−lysine (LK) peptides at interfaces.[27] For one unbiased result, Ca ions were randomly placed into the simulation box, with the initial snapshots shown in Figure S8. After simulation, Ca^{2+} ions were highly coordinated into interfacial peptides due to their strong interaction. A closer look (inset in Figure 3B) shows that each Ca^{2+} ion was chelated by two glutamic acid sites, which is in good agreement with the Calcium complexation ratio within the CaC_2O_4 sheet as determined from our XPS analysis. Here, the chelated Ca^{2+} ions, acting as the salt bridge, drive the backbones to "curl" and fold back on themselves, leading to more turn-like secondary structures, which is in agreement with our SFG band assignment.

We calculated theoretical SFG spectra of the amide I band over 200 frames from 100 to 500 ns in 2 ns steps for the four simulations, according to the formalism described in ref 28 (see the SI for more details). In calculations, the hydrogen bond-induced local-mode frequency shifts are modeled via the correlation found by Cho et al. among factors including the strength of the accepted and/or donated hydrogen bond(s), the C═O length in the amide groups, and the local-mode amide I frequency.[29] Specifically, we take the C═O length from the coordinates and apply the equation $\nu = \nu_0 + \alpha\delta r_{CO}$, where ν_0 is the base frequency, α is the proportionality constant, and δr_{CO} is the deviation of the carbon−oxygen bond from its equilibrium value, which was 1.229 Å for amide groups with secondary amines. The optimal match with the experimental spectra was found with α = 1000 and ν_0 = 1622 cm^{-1}. The calculated amide I spectra, as presented in Figure 2C,D, capture the band positions, spectral shape, and intensity increase observed for the amide I band in the experiments. The gradual appearance of a small band at ∼1690 cm^{-1} in Figure 2A,B is not visible in the calculated spectra; this high-frequency mode is related to the aggregated β-turns from many peptide monomers, which can not be formed by the limited peptides as placed in the simulation box. However, the generally good agreement between calculation and experiment lends credence to simulation and prompted us to perform further analysis. Non-classical crystallization theories suggest that the Ca^{2+} ions coordinated by peptide side chains may template the CaC_2O_4 lattice and steer its growth within the sheet.[15,30] We calculate the radial distribution function (RDF) of Ca^{2+} ions (Figure 3C), which shows a dominant peak near 4 Å. Comparing this number with the calcium spacing within the Calcium oxalate mono- (COM) and dihydrate (COD) polymorphs, it becomes clear that, while the calcium spacing is smaller in COM, there is a remarkable match of the Ca^{2+} ion spacing within the peptide layer with the calcium spacing in COD. The MD simulations therefore suggest that LE10 peptides can effectively stabilize COD. Indeed, SEM images of the sheets collected after extended assembly times show the octahedral crystal shapes expected for COD (Figure S2). While X-ray diffraction (XRD) measurements of the sheets have not yielded a diffraction signal, we have analyzed the crystal structure of CaC_2O_4 precipitated by LE10 in bulk solution. the XRD pattern further supports COD polymorph production by LE10 peptides (Figures S4 and S5).

In conclusion, using a facile approach, we have successfully fabricated CaC_2O_4 nanosheets by employing biomimetic β-sheet LE10 peptides assembled at the air−water interface. The obtained nanosheets are freestanding with defect-free areas exceeding 50 × 50 μm^2. Combined SFG and molecular

DOI: 10.1021/acs.jpclett.9b00684
J. Phys. Chem. Lett. 2019, 10, 2170−2174

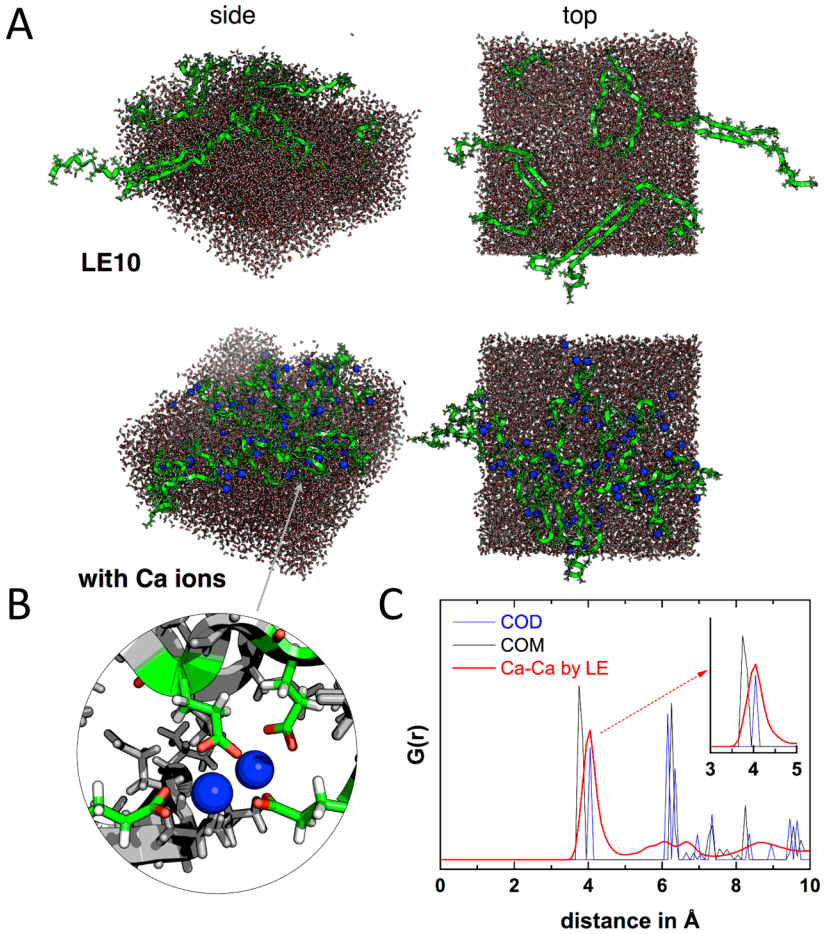

Figure 3. (A) Snapshots of MD simulations after 100 ns without and with Ca^{2+} ions. (B) Detailed view of glutamic acid side chains chelating Ca ions. Color scheme for rendered images: Ca ions, blue; peptide backbone, green; oxygen, red. (C) Radial distribution function $G(r)$ of the Ca−Ca distance within the simulations (red). $G(r_{Ca-Ca})$ from crystal structure data for oxalate structures COM (black) and COD (blue) are also shown (see the main text for details).

dynamics simulation studies indicate that the nanosheet formation is enabled by the key interplay between peptides and Ca^{2+} ions: binding of the Ca^{2+} ions refines the peptide's structural motif, which in turn templates the Ca^{2+} ions to nucleate the CaC_2O_4 nanosheet by matching the COD lattice. The study shows that the inclusion of ion interactions in the design of functional peptides will be important for the design and fabrication of 2D inorganic biomimetic mineral nanosheets. This strategy could potentially be used to design mineral sheets using related templating molecules such as peptoids and block copolymers.

■ ASSOCIATED CONTENT

Supporting Information

The Supporting Information is available free of charge on the ACS Publications website at DOI: 10.1021/acs.jpclett.9b00684.

Description of experimental procedures, more characterization on XRD, SEM, TEM, and XPS, description of SFG analysis and fitting parameters, description of MD simulations and SFG spectra calculation (PDF)

■ AUTHOR INFORMATION

Corresponding Author

*E-mail: lu@mpip-mainz.mpg.de.

ORCID

Hao Lu: 0000-0002-7338-2295
Helmut Lutz: 0000-0002-7915-8542
Steven J. Roeters: 0000-0003-3238-2181
Ingo Lieberwirth: 0000-0003-1323-524X
Rafael Muñoz-Espí: 0000-0002-8146-2332
Mischa Bonn: 0000-0001-6851-8453
Tobias Weidner: 0000-0002-7083-7004

Notes

The authors declare no competing financial interest.

■ ACKNOWLEDGMENTS

The authors greatly thank Elke Muth for the peptide synthesis and Michael Steiert for XRD measurements. SEM and TEM support by Gunnar Glasser and Katrin Kirchhoff is gratefully acknowledged. We gratefully acknowledge Helma Burg and Rüdiger Berger for AFM support. S.J.R. and T.W. are grateful for discussions about SFG spectra averaging with Dr. Sean A. Fischer. R.M.E. acknowledges financial support from the Spanish Ministry of Economy and Competitiveness through a Ramón y Cajal grant (Grant No. RYC-2013-13451) and from the Max Planck Society through funding of the Max Planck Partner Group on Colloidal Methods for Multifunctional Materials (CM3) at the University of Valencia. T.W. thanks the Deutsche Forschungsgemeinschaft (WE4478/4-1)

DOI: 10.1021/acs.jpclett.9b00684
J. Phys. Chem. Lett. 2019, 10, 2170−2174

and the Aarhus University Research Foundation (AUFF) for financial support.

REFERENCES

(1) Turchanin, A.; Golzhauser, A. Carbon Nanomembranes. *Adv. Mater.* **2016**, *28*, 6075−6103.
(2) Zhao, H. W.; Zhu, Y. J.; Li, F. S.; Hao, R.; Wang, S. X.; Guo, L. A Generalized Strategy for the Synthesis of Large-Size Ultrathin Two-Dimensional Metal Oxide Nanosheets. *Angew. Chem., Int. Ed.* **2017**, *56*, 8766−8770.
(3) Mann, S. *Biomineralization: Principles and Concepts in Bioinorganic Materials Chemistry*; Oxford University Press: Oxford, 2001.
(4) Suzuki, M.; Saruwatari, K.; Kogure, T.; Yamamoto, Y.; Nishimura, T.; Kato, T.; Nagasawa, H. An Acidic Matrix Protein, Pif, Is a Key Macromolecule for Nacre Formation. *Science* **2009**, *325*, 1388−1390.
(5) Schrettl, S.; et al. Functional Carbon Nanosheets Prepared from Hexayne Amphiphile Monolayers at Room Temperature. *Nat. Chem.* **2014**, *6*, 468−476.
(6) Anselmetti, D.; Golzhauser, A. Converting Molecular Monolayers into Functional Membranes. *Angew. Chem., Int. Ed.* **2014**, *53*, 12300−12302.
(7) Robertson, E. J.; Battigelli, A.; Proulx, C.; Mannige, R. V.; Haxton, T. K.; Yun, L. S.; Whitelam, S.; Zuckermann, R. N. Design, Synthesis, Assembly, and Engineering of Peptoid Nanosheets. *Acc. Chem. Res.* **2016**, *49*, 379−389.
(8) Robertson, E. J.; Olivier, G. K.; Qian, M.; Proulx, C.; Zuckermann, R. N.; Richmond, G. L. Assembly and Molecular Order of Two-Dimensional Peptoid Nanosheets through the Oil-Water Interface. *P. Natl. Acad. Sci. USA* **2014**, *111*, 13284−13289.
(9) Qin, H. L.; Li, F. J.; Wang, D.; Lin, H. Z.; Jin, J. Organized Molecular Interface-Induced Noncrystallizable Polymer Ultrathin Nanosheets with Ordered Chain Alignment. *ACS Nano* **2016**, *10*, 948−956.
(10) Lu, H.; Lutz, H.; Roeters, S. J.; Hood, M. A.; Schafer, A.; Munoz-Espi, R.; Berger, R.; Bonn, M.; Weidner, T. Calcium-Induced Molecular Rearrangement of Peptide Folds Enables Biomineralization of Vaterite Calcium Carbonate. *J. Am. Chem. Soc.* **2018**, *140*, 2793−2796.
(11) Lutz, H.; Jaeger, V.; Schmüser, L.; Bonn, M.; Pfaendtner, J.; Weidner, T. The Structure of the Diatom Silaffin Peptide R5 within Freestanding Two-Dimensional Biosilica Sheets. *Angew. Chem., Int. Ed.* **2017**, *56*, 8277−8280.
(12) Qiu, S. R.; Wierzbicki, A.; Orme, C. A.; Cody, A. M.; Hoyer, J. R.; Nancollas, G. H.; Zepeda, S.; De Yoreo, J. J. Molecular Modulation of Calcium Oxalate Crystallization by Osteopontin and Citrate. *Proc. Natl. Acad. Sci. U. S. A.* **2004**, *101*, 1811−1815.
(13) Chien, Y. C.; Masica, D. L.; Gray, J. J.; Nguyen, S.; Vali, H.; Mckee, M. D. Modulation of Calcium Oxalate Dihydrate Growth by Selective Crystal-Face Binding of Phosphorylated Osteopontin and Polyaspartate Peptide Showing Occlusion by Sectoral (Compositional) Zoning. *J. Biol. Chem.* **2009**, *284*, 23491−23501.
(14) Delmonte, M.; Sabbioni, C.; Zappia, G. The Origin of Calcium Oxalates on Historical Buildings, Monuments and Natural Outcrops. *Sci. Total Environ.* **1987**, *67*, 17−39.
(15) Ruiz-Agudo, E.; Burgos-Cara, A.; Ruiz-Agudo, C.; Ibanez-Velasco, A.; Colfen, H.; Rodriguez-Navarro, C. A Non-Classical View on Calcium Oxalate Precipitation and the Role of Citrate. *Nat. Commun.* **2017**, *8* (1−10), 768.
(16) Shen, Y. R. *The Principles of Nonlinear Optics*; J. Wiley: New York, 1984.
(17) Lambert, A. G.; Davies, P. B.; Neivandt, D. J. Implementing the Theory of Sum Frequency Generation Vibrational Spectroscopy: A Tutorial Review. *Appl. Spectrosc. Rev.* **2005**, *40*, 103−145.
(18) Roy, S.; Covert, P. A.; FitzGerald, W. R.; Hore, D. K. Biomolecular Structure at Solid-Liquid Interfaces as Revealed by Nonlinear Optical Spectroscopy. *Chem. Rev.* **2014**, *114*, 8388−8415.
(19) Ding, B.; Jasensky, J.; Li, Y.; Chen, Z. Engineering and Characterization of Peptides and Proteins at Surfaces and Interfaces: A Case Study in Surface-Sensitive Vibrational Spectroscopy. *Acc. Chem. Res.* **2016**, *49*, 1149−1157.
(20) Paszti, Z.; Guczi, L. Amino Acid Adsorption on Hydrophilic TiO_2: A Sum Frequency Generation Vibrational Spectroscopy Study. *Vib. Spectrosc.* **2009**, *50*, 48−56.
(21) Mudunkotuwa, I. A.; Minshid, A. A.; Grassian, V. H. ATR-FTIR Spectroscopy as a Tool to Probe Surface Adsorption on Nanoparticles at the Liquid-Solid Interface in Environmentally and Biologically Relevant Media. *Analyst* **2014**, *139*, 870−881.
(22) Nguyen, K. T.; King, J. T.; Chen, Z. Orientation Determination of Interfacial Beta-Sheet Structures in Situ. *J. Phys. Chem. B* **2010**, *114*, 8291−8300.
(23) Singh, B. R. *Infrared Analysis of Peptides and Proteins: Principles and Applications*; American Chemical Society: Washington, DC, 2000.
(24) Hilario, J.; Kubelka, J.; Keiderling, T. A. Optical Spectroscopic Investigations of Model Beta-Sheet Hairpins in Aqueous Solution. *J. Am. Chem. Soc.* **2003**, *125*, 7562−7574.
(25) Fu, L.; Ma, G.; Yan, E. C. Y. In Situ Misfolding of Human Islet Amyloid Polypeptide at Interfaces Probed by Vibrational Sum Frequency Generation. *J. Am. Chem. Soc.* **2010**, *132*, 5405−5412.
(26) Fu, L.; Liu, J.; Yan, E. C. Y. Chiral Sum Frequency Generation Spectroscopy for Characterizing Protein Secondary Structures at Interfaces. *J. Am. Chem. Soc.* **2011**, *133*, 8094−8097.
(27) Baio, J. E.; Zane, A.; Jaeger, V.; Roehrich, A. M.; Lutz, H.; Pfaendtner, J.; Drobny, G. P.; Weidner, T. Diatom Mimics: Directing the Formation of Biosilica Nanoparticles by Controlled Folding of Lysine-Leucine Peptides. *J. Am. Chem. Soc.* **2014**, *136*, 15134−15137.
(28) Roeters, S. J.; van Dijk, C. N.; Torres-Knoop, A.; Backus, E. H. G.; Campen, R. K.; Bonn, M.; Woutersen, S. Determining in Situ Protein Conformation and Orientation from the Amide-I Sum-Frequency Generation Spectrum: Theory and Experiment. *J. Phys. Chem. A* **2013**, *117*, 6311−6322.
(29) Ham, S.; Kim, J. H.; Lee, H.; Cho, M. H. Correlation between Electronic and Molecular Structure Distortions and Vibrational Properties. II. Amide I Modes of NMA-nD_2O Complexes. *J. Chem. Phys.* **2003**, *118*, 3491−3498.
(30) Gebauer, D.; Volkel, A.; Colfen, H. Stable Prenucleation Calcium Carbonate Clusters. *Science* **2008**, *322*, 1819−1822.

DOI: 10.1021/acs.jpclett.9b00684
J. Phys. Chem. Lett. 2019, 10, 2170−2174